J. Fluid Mech. (1998), *vol.* 358, *pp.* 223–244. Printed in the United Kingdom

© 1998 Cambridge University Press

The response of sheared turbulence to changes in curvature

By B. CHEBBI[1], A. G. L. HOLLOWAY[2] AND S. TAVOULARIS[1]

[1]Department of Mechanical Engineering, University of Ottawa, Ottawa, Ont. K1N 6N5, Canada

[2]Department of Mechanical Engineering, University of New Brunswick, Fredericton, N.B. E3B 5A3, Canada

(Received 5 December 1994 and in revised form 9 September 1997)

Transversely homogeneous, uniformly sheared, turbulent flow was allowed to reach its asymptotic structure in a straight wind tunnel section and then it was passed through a sequence of two curved sections and a final straight section. The cross-sectional shape of the entire wind tunnel was rectangular, while the two curved sections had circular centrelines with the same radius but opposing curvatures. In all cases, the mean strain rate due to curvature was relatively weak ($\pm 5\%$), compared to the mean shear rate, but its effects on the turbulence kinetic energy and structure were substantial; streamwise pressure gradient effects were negligible. The turbulence structure approached approximately self-similar states towards the downstream ends of each curved section but the main interest of the present study was the rate of adjustment of the turbulence following a stepwise change in curvature. It has been shown that the adjustment of the shear stress anisotropy, which is a sensitive indicator of structural changes, can be approximated by a first-order system response, whose time constant scales with the inverse mean shear and is independent of the curvature parameter. Uniformly sheared flow results were used for an interpretation of the structure of curved turbulent boundary layers, both during adjustment and in a fully developed state.

1. Introduction

Streamline curvature in the plane of the mean shear is one of the most important sources of mean straining in turbulent shear flows. Its effect on the turbulence structure is known to be significant and, for this reason, it has been studied extensively. A qualitative assessment of this effect can be based on an analogy to linear stability theory, which has identified the radial distribution of the mean angular momentum as a primary factor in establishing whether the flow is stable or not. Previous work has demonstrated that, when the mean angular momentum increases with increasing radius of curvature, the turbulence would be suppressed, in which case the curvature is referred to as 'stabilizing' while, when the mean angular momentum decreases with increasing radius of curvature, the turbulence would be enhanced, and the curvature is referred to as 'destabilizing'. Thus, compared to a plane wall, a convex wall would have a stabilizing influence on a turbulent boundary layer, while a concave wall would have a destabilizing influence on it.

The present study is concerned with the structural changes of sheared turbulence subjected to stepwise changes of flow curvature. Both the magnitude of this structural

https://doi.org/10.1017/S0022112097008185 Published online by Cambridge University Press

change as well as the rate of adjustment to a new structure have been investigated. Both aspects have been the subject of numerous experimental and analytical studies. An early critical review of curvature effects was compiled by Bradshaw (1973), who concluded that prolonged application of a small additional mean strain rate, $e = \overline{U}/R$ ($\overline{U}$ is the mean velocity and R is the radius of curvature), although possibly introducing a negligible change in the total strain rate, could cause a substantial change in the Reynolds stresses. He proposed that the change in stresses, compared to those in a corresponding rectilinear flow, would be as large as if their production were multiplied by the factor $1 + \alpha e/(\partial\overline{U}/\partial n)$, where n is a direction normal to the mean velocity and the coefficient α is of the order of 10. Bradshaw further deduced that Prandtl's mixing length theory would be approximately valid in curved boundary layers, if the mixing length were multiplied by the above factor; he estimated the values $\alpha \approx 14$ for a convex wall and $\alpha \approx 8$ for a concave wall. Most available turbulence measurements in curved shear flows were performed after Bradshaw's review was published and they generally confirmed his basic premises and his order of magnitude estimate for α (Holloway & Tavoularis 1992, hereafter referred to as HT).

The rate of adjustment of the turbulent structure to stepwise changes in curvature was also studied by Bradshaw (1973), who conjectured that, following a stepwise application of a constant extra strain rate, e, the value of the parameter α required to optimize agreement with the experimental results would rise exponentially to an asymptotic value. Bradshaw's estimate of the 'time constant' of exponential adjustment for boundary layers with a thickness δ was 10δ. This subject has been discussed by Gillis & Johnston (1980, 1983), Gibson, Verriopoulos & Vlachos (1984), Muck, Hoffmann & Bradshaw (1985), Hoffman, Muck & Bradshaw (1985) and Barlow & Johnston (1988). The reverse phenomenon, namely recovery of the turbulence from curvature, which is also important in practical applications, has been investigated by several authors. Smits, Young & Bradshaw (1979) studied the relaxation of turbulent boundary layers subjected to short regions of strong convex and concave curvatures, while Gillis & Johnston (1980, 1983), Alving & Smits (1986) and Alving, Smits & Watmuff (1990) studied the recovery of a turbulent boundary layer from prolonged strong convex curvature. Recovery from prolonged concave curvature appears not to have been studied.

These results provided some support for Bradshaw's analysis, but also introduced much additional detail. In particular, it was observed that the turbulence structure, as measured by turbulence stress ratios, adjusts to onset or removal of both types of curvature quite rapidly, typically within a few δ. On the other hand, the adjustments of the mean velocity and turbulence profiles require greater distances, which appear to depend on the types of curvature and its change. This adjustment length was found to be about 15δ for the onset of convex curvature and from 15δ to 90δ for recovery from it. The adjustment to onset of concave curvature, even for boundary layers not seriously contaminated by strong quasi-steady longitudinal vortices, tends to be slower than that for convex layers. When such vortices exist, the resulting three-dimensional flow has a substantially longer adjustment length.

Curvature reversal is a more drastic configuration than the types of curvature change described above, albeit also common in applications. Baskaran, Smits & Joubert (1987, 1991) examined in detail the development of a turbulent boundary layer over a curved hill, which included successive plane, concave and convex wall regions. In this experiment, two extra strain rates were present, one due to streamline curvature and another due to the streamwise pressure gradient; both were strong and, in places, comparable in magnitude to the mean strain rate due to shearing.

https://doi.org/10.1017/S0022112097008185 Published online by Cambridge University Press

An inspection of the Reynolds stress equations, however, showed that the interaction between these two effects would be rather weak, because the curvature had a stronger effect on the shear stress than on the normal stresses, while the effects of pressure gradient mainly appeared through the production of normal stresses.

These authors also discussed the development of an internal layer, whose initiation was attributed to the abrupt change in curvature. More recently, Bandyopadhyay & Ahmed (1993) performed a comparative study of the development of two boundary layers subjected to sequences of convex–concave and concave–convex longitudinal surface curvatures. Their measurements included wall pressure, skin friction, mean velocity and streamwise turbulence intensity. These flows were also subjected to a streamwise pressure gradient, but the authors concluded that its effects would be secondary to those of curvature. A main observation in this study was the asymmetric response of the turbulent boundary layer to concave and convex surface curvatures, manifested by differences in the skin friction in the plane recovery region: this skin friction was lower following a sequence of concave–convex curvature than that following a corresponding sequence of convex–concave curvature.

Uniformly sheared, essentially unbounded, nearly homogeneous turbulence (USF) was successfully generated in curved ducts by HT (see also Holloway & Tavoularis 1993). This flow configuration is unique because it allows a study of curvature effects without the complications created by walls and entrainment. A study of turbulence model performance in this flow was conducted by Gatski & Savill (1989). HT were mostly concerned with the fully developed USF structure, following exposure to prolonged uniform curvature, and they produced asymptotic relationships among various structural parameters, notably the Reynolds shear stress and the relative strength of curvature.

The present investigation is focused on the region of adjustment of USF structure, following stepwise changes in the mean curvature of the wind tunnel, including transition from a rectilinear to a curved section, curvature reversal and relaxation from a curved to a rectilinear section. Our main objective is to determine the rate of adjustment of the flow structure and its possible dependence upon the type and magnitude of curvature change. Our intention was to minimize and, if possible, to eliminate the undesirable effects of boundary layers developing along the four wind-tunnel walls and those of streamwise pressure gradients that would inevitably appear following curvature changes. The present USF results are consistent with Bradshaw's analysis and, in spite of the absence of any direct wall effects, consistent with many observations previously made in the outer regions of curved boundary layers.

2. Analytical considerations

The present study is concerned with flows which are two-dimensional, on the average, so that their mean streamlines are plane curves, and such that their lateral extent is small compared to their streamwise extent. The adopted coordinate system (s, n, z), shown in figure 1, is a modified version of a general curvilinear coordinate system, such that the coordinate s follows a plane curve, called the 'centreline', the coordinate n is along a straight axis, normal to the centreline, and the coordinate z is normal to the plane of the centreline and conforming with the right-hand rule. It will be assumed that $n = 0$ on the centreline and, for consistency with the usual boundary layer convention, n will be considered positive if it points towards the direction of increasing mean velocity, assumed not to reverse throughout the flow. For compatibility with the HT experiments, we shall adopt the convention that the

https://doi.org/10.1017/S0022112097008185 Published online by Cambridge University Press

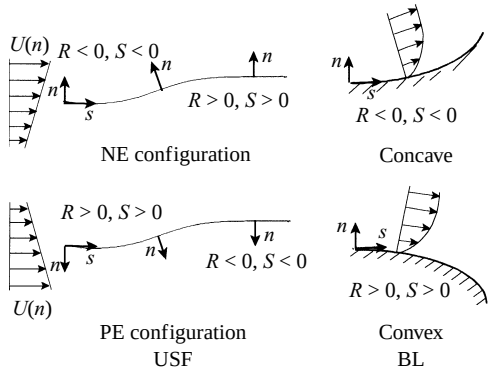


FIGURE 1. Definition of the coordinate systems in curved uniformly sheared flows and curved boundary layers. The z-axis is defined normal to the shown plane, according to the right-hand rule.

radius of curvature, R_c, of the centreline will be considered as positive when the centre of curvature is towards negative n and negative otherwise. In this coordinate system, the velocity components will be denoted as (U, V, W) and, following the usual convention, overbars will denote averages and lower-case symbols will denote fluctuations.

Now, consider a stationary turbulent flow, with a constant mean velocity gradient $\partial\overline{U}/\partial n$ (within the present approximation, the dependence of $\overline{U}$ on s will be assumed to be very weak), homogeneous on any (n, z)-plane, and such that the scale of turbulent motions is small compared to the distance from the centreline to any solid boundary or turbulent/non-turbulent interface. The local curvature parameter (HT) will be defined as

$$S = \frac{\overline{U}_c/R_c}{\partial\overline{U}/\partial n}. \tag{2.1}$$

It is clear that S would be positive or negative, depending on the orientations of the mean shear rate and the curvature. The two configurations of the present experiment have been identified in figure 1: NE indicates a configuration in which $S < 0$ at the start, and PE a configuration in which $S > 0$ at the start.

Then, the equations describing the evolution of the turbulent kinetic energy per unit mass, $\frac{1}{2}q^2 = \frac{1}{2}(\overline{u^2} + \overline{v^2} + \overline{w^2})$, and the non-vanishing turbulent stresses can be simplified to the following forms:

$$\overline{U}\frac{\mathrm{d}(\frac{1}{2}q^2)}{\mathrm{d}s} = P - \epsilon, \tag{2.2}$$

$$\overline{U}\frac{\mathrm{d}(\frac{1}{2}\overline{u^2})}{\mathrm{d}s} = -\overline{uv}\frac{\partial\overline{U}}{\partial n}(1+S) + \phi_{uu} - \epsilon_{uu}, \tag{2.3}$$

$$\overline{U}\frac{\mathrm{d}(\frac{1}{2}\overline{v^2})}{\mathrm{d}s} = 2\overline{uv}\frac{\partial\overline{U}}{\partial n}S + \phi_{vv} - \epsilon_{vv}, \tag{2.4}$$

$$\overline{U}\frac{\mathrm{d}(\frac{1}{2}\overline{w^2})}{\mathrm{d}s} = \phi_{ww} - \epsilon_{ww}, \tag{2.5}$$

$$\overline{U}\frac{\mathrm{d}(\overline{uv})}{\mathrm{d}s} = -\overline{v^2}\frac{\partial\overline{U}}{\partial n}(1+S) + 2\overline{u^2}\frac{\partial\overline{U}}{\partial n}S + \phi_{uv} - \epsilon_{uv}, \tag{2.6}$$

https://doi.org/10.1017/S0022112097008185 Published online by Cambridge University Press

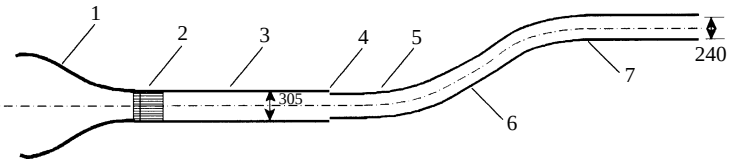


FIGURE 2. Sketch of the experimental facility. 1, contraction; 2, shear generator/flow separator; 3, straight section; 4, boundary layer bleeding; 5, start of curved subsection; 6, curvature reversal; 7, start of straight recovery subsection. Dimensions in mm.

where the production, P, of the turbulent kinetic energy is defined as

$$P = -\overline{uv}\frac{\partial \overline{U}}{\partial n}(1 - S). \tag{2.7}$$

ϵ is the dissipation rate, partitioned into the components ϵ_{uu}, ϵ_{vv} and ϵ_{ww}, and ϕ_{uu}, ϕ_{vv}, ϕ_{ww} and ϕ_{uv} are the pressure strain-rate covariances. These equations are identical to those derived by HT for uniform curvature, and consistent with those derived by Gatski & Savill (1989). It may be remarked that the above equations can be integrated to yield continuous distributions of the Reynolds stresses even at locations of discontinuous change, including reversal, of curvature. In such cases, however, one might expect that the omitted streamwise diffusion terms should act to smooth the apparent discontinuities in the derivatives of the stresses. By letting $R_c \to \infty$, and thus $S \to 0$, the above equations are reduced to the corresponding forms for rectilinear USF (Harris, Graham & Corrsin 1977).

3. Experimental apparatus and instrumentation

3.1. *The wind tunnel facility*

The wind tunnel used in the present experiments was located at the University of Ottawa; its main features are shown schematically in figure 2. The initial straight test section was nominally 305 mm high, 457 mm wide and 3190 mm long. At its upstream end, it was equipped with a shear generator and a flow separator. The shear generator was 150 mm long and comprised 12 separate, 25.4 mm high, channels. Sets of different screens with various solidities were stretched across these channels to introduce a variable flow resistance, as required to create a uniformly sheared flow. The flow separator, 610 mm long and consisting of 12 channels aligned with those in the shear generator, was inserted to improve the transverse homogeneity of the large scales. A nearly homogeneous shear flow was produced in this tunnel, having a value of the shear generator constant

$$k_s = \frac{1}{\overline{U}_c}\frac{\partial \overline{U}}{\partial n} \approx 6.2 \text{ m}^{-1} \tag{3.1}$$

for centreline speeds $\overline{U}_c$ ranging from 5 to 15 m s^{-1}. The wind tunnel design and operation have been described in more detail by Karnik & Tavoularis (1987).

The flow exiting the initial straight section was passed through a compound curved section, which consisted of a straight entrance subsection, 203 mm long, a first curved subsection with a centreline arclength of 1017 mm, a second curved subsection of equal length but reversed curvature, and a final straight subsection, 1245 mm long. The origin of the coordinate s was at the start of the first straight subsection, so that $s = 203$ mm at the start of curvature. The centreline radii of curvature of both

https://doi.org/10.1017/S0022112097008185 Published online by Cambridge University Press

curved subsections were 3500 mm. For this radius, and for a centreline velocity of 10 m s^{-1}, the curvature parameter was $S \approx \pm 0.05$. The compound curved section was also rectangular, but both its height and its width were smaller than those at the exit of the initial straight section. The inlet to the curved section was positioned to face the core of the incoming flow and such that the boundary layers developing along the four walls of the initial straight section were passively (i.e. without suction or other forcing) bled into the room. Care was taken to sharpen the leading edges of the curved section in order to reduce the chance of separation. The boundary layer characteristics before and after bleeding were not investigated in detail, not being of great importance in this study. However, velocity measurements just after the entrance of the compound curve section confirmed that the incoming flow was essentially homogeneous. The height of the compound curved channel, which was kept constant at $h = 240$ mm, will be used for non-dimensionalizing the transverse coordinate. The channel's width was gradually increased from 413 mm to 430 mm as partial compensation for boundary layer growth.

To align the straight and curved sections, their centrelines were engraved on the sidewalls and adjusted to be tangent at their interseaction. To align the probe with the flow direction, circumferential and radial lines were engraved on the two sidewalls of the section. The axis of the traversing mechanism was offset so that the tip of the probe would traverse radially.

3.2. *Measuring instrumentation and uncertainty*

Hot-wire instrumentation. The turbulence measurements were conducted with a commercial hot-wire probe (TSI, model 1248 BJ-T1.5), having two sensors made of tungsten and arranged in a cross-wire configuration, inclined by $\pm 45^\circ$ (nominally) with respect to the probe axis. The two sensing elements had diameters of 5 μm and lengths of 1.2 mm, and were separated by a distance of 0.50 mm. The uncertainties in the sensor orientation with respect to the probe axis (determined by direct calibration over a probe angle range of $\pm 30^\circ$) and in the probe orientation with respect to the wind tunnel centreline (determined with a precision cathetometer) were estimated to be about $\pm 0.5^\circ$. The hot-wire signals were conditioned by off-setting, amplification and low-pass filtering at 10 kHz, digitized at rates of 2 kHz and 25 kHz, and stored on magnetic tapes for later processing. Typically, 50 data records, each with two sets of 2048 samples, were used to calculate the turbulence statistics at each location. The 2 kHz data were used to calculate the turbulent stresses, while the 25 kHz data were used to calculate the time-derivative statistics. The analog to digital converter (Data Translation, model DT2828) could sample four channels simultaneously with 12 bits of resolution.

Spatial resolution of the probe. The sensor length was typically about 4% of the streamwise integral length scale, about 20% of the streamwise Taylor microscale and about 8.5 times the estimated Kolmogorov microscale. Using Corrsin's (1963) method, one may infer that a systematic underestimation of the order of 0.5% could occur in the turbulent kinetic energy and the Reynolds stresses, due to the limited spatial resolution of the probe. This error is negligible compared to the random uncertainty. On the other hand, Wyngaard's (1969) analysis for the present conditions leads to an underestimation of the order of 30% for the mean-squared temporal velocity derivative, which results in an overestimation of the order of 20% for the Taylor microscale, λ. For this reason, direct Taylor microscale measurements are not reported here and the turbulent kinetic energy dissipation rate is estimated from the simplified turbulent kinetic energy equation.

https://doi.org/10.1017/S0022112097008185 Published online by Cambridge University Press

Overall uncertainty of the measurements. An analysis of cross-wire uncertainty, conforming to current international standards, has been performed. It accounts for the uncertainties in curve-fitting of calibration data to King's law and in the determination of sensor and probe body orientations, which are the main contributors to the uncertainty of first and second velocity moments. The resulting typical uncertainties within a confidence level of 95% (i.e. with 20:1 odds that the true value would be inside the corresponding interval, centred about the reported values) are as follows (the shear stress correlation coefficient, ρ, and the shear stress anisotropy, m_{uv}, will be defined in §4.2):

$$\delta\overline{U}/\overline{U} \approx \pm 2\%,\ \delta\overline{V}/\overline{U} \approx \pm 3\%,\ \delta\overline{W}/\overline{U} \approx \pm 3\%$$
$$\delta\overline{u^2}/\overline{u^2} \approx \pm 4\%,\ \delta\overline{v^2}/\overline{v^2} \approx \pm 8\%,\ \delta\overline{w^2}/\overline{w^2} \approx \pm 8\%,\ \delta\overline{q^2}/\overline{q^2} \approx \pm 3\%$$
$$\delta\overline{uv}/\overline{uv} \approx \pm 8\%,\ \delta\rho \approx \pm 0.03, \delta m_{uv} \approx \pm 0.01.$$

4. Measurements

4.1. *Mean flow*

The centreline velocity at the entrance to the compound curved section was set to about 10 m s^{-1}. Two flow configurations were obtained, depending on whether the shear generator was in its upright or an inverted orientation. For consistency with the convention illustrated in figure 1, the coordinate n at the entrance to the compound section was defined as pointing towards the direction of increasing velocity, i.e. it had different directions for the two configurations. As explained in §2, these configurations will be referred to as NE and PE, depending on whether the parameter S was negative or positive at the entrance to the first curved subsection (figure 1). Measurements of the components of the mean velocity along the centreline of the test section showed that the maximum variation of the streamwise component, $\overline{U}_c$, was 6% for the PE configuration and 10% for the NE configuration, while the transverse and spanwise components were generally less than 4% of U_c. Such deviations from an idealized velocity field can be considered as mild; they can be mostly attributed to residual boundary layer growth, despite the slight divergence of the sidewalls, and to possible mean streamline divergence from the geometric centreline due to the unequal boundary layer thicknesses along the four walls. The streamwise velocity variation can be associated with a mild streamwise pressure gradient, whose effects were estimated to be small compared to those of curvature (see discussion in §5.1).

Transverse profiles of the streamwise velocity, taken at four different streamwise stations, are shown in figure 3. The variation of the slopes of the profiles was relatively small but systematic and can be attributed partly to the flow turning. Inviscid flow analysis, conserving the mean vorticity, $(\partial\overline{U}/\partial n)(1+S)$, of the flow, predicts that entry of a shear flow into a section with a larger S would tend to decrease the mean shear, while the opposite would happen if S decreased. The gradual deterioration of the slope of the profiles over the length of the tunnel is mainly attributed to boundary layer development along the four walls. Typically, the mean shear magnitude was about 65 s^{-1} at the entrance to the compound curved section and, by the end of the second curved subsection, it decreased to about 55 s^{-1} for PE and 50 s^{-1} for NE. This introduced some difference between the nominal total strain, $\tau = |k_s|s$, and that estimated from the local values of the shear parameter, k_s. Such differences were quite small for the PE configuration but exceeded 10% at the end of the second curved subsection for the NE configuration. The development

https://doi.org/10.1017/S0022112097008185 Published online by Cambridge University Press

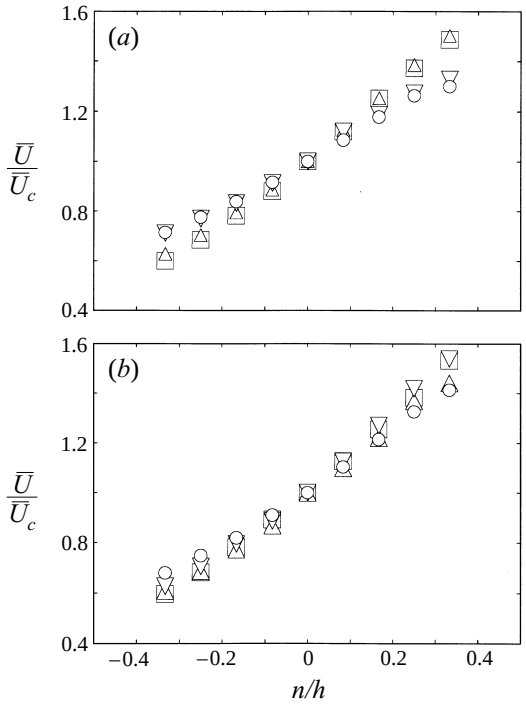


FIGURE 3. Transverse profiles of the dimensionless streamwise mean velocity, $\overline{U}/\overline{U}_c$. (*a*) configuration NE; (*b*) configuration PE. $s/h = 0.6$ (□), 3.0 (△), 7.0 (▽), 10.8 (○).

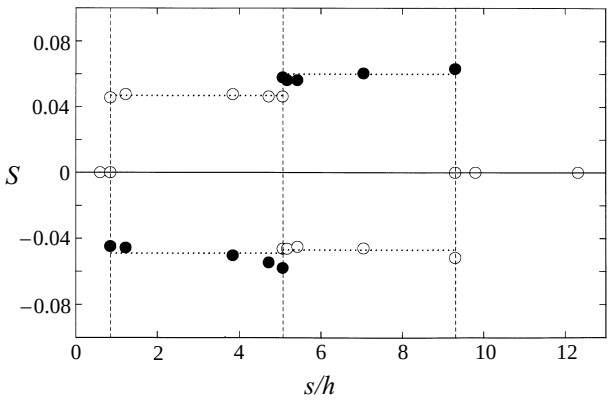


FIGURE 4. Variation of the curvature parameter, S, along the centreline for configurations NE (●) and PE (○). Vertical dashed lines indicate the locations of curvature change, while dotted lines indicate the average values of S within each curved subsection.

of the parameter S along the wind tunnel's centreline is shown in figure 4. The variations of the magnitudes of the mean shear and the S parameter along each curved subsection may be viewed as small, when compared to the sudden changes in S at the boundaries between subsections, which were either 100% or 200%. This permitted the use of the following nominal values of S for each pair of curved subsections: −0.049 and 0.060 for the NE configuration and 0.047 and −0.047 for the PE configuration.

https://doi.org/10.1017/S0022112097008185 Published online by Cambridge University Press

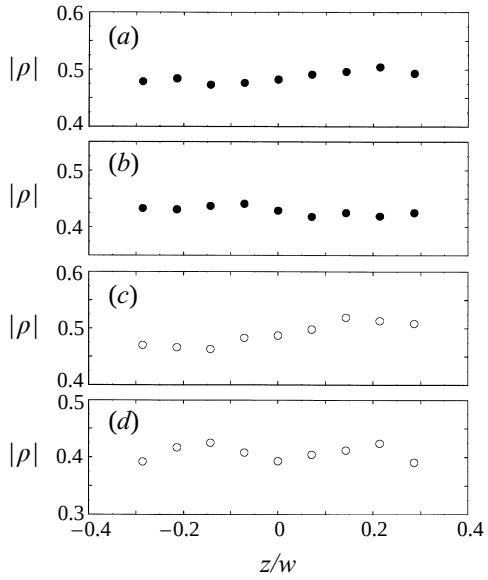


FIGURE 5. Spanwise profiles of the shear stress correlation coefficient (in absolute value) at $n/h = 0$ for configurations NE (●) and PE (○). (*a,c*) $s/h = 0.6$; (*b,d*) $s/h = 11.9$. $w = 413$ mm is the initial test section width.

4.2. *Reynolds stresses and evolution of anisotropy*

The transverse and spanwise inhomogeneities of the Reynolds stresses were relatively mild and comparable to those in previous USF studies (HT). For example, figure 5 shows that the levels of spanwise inhomogeneity of the shear stress correlation coefficient, $\rho = \overline{uv}/u'v'$, near the beginning and the end of the test section for both NE and PE configurations were relatively weak, and did not appear to change systematically when changes of curvature occurred. This is consistent with the lack of other detectable signs of streamwise vortices in the central core of the flow, although one may not exclude the possibility of formation of such vortices near the concave wall. Consistent with the HT results, the rate of growth of the Reynolds stresses was enhanced for $S < 0$ and suppressed for $S > 0$, in comparison to its rectilinear flow levels (figure 6).

The changes in the normal dimensionless Reynolds stress anisotropies, m_{uu}, m_{vv} and m_{ww} (defined as $m_{uu} = \overline{u^2}/q^2 - 1/3$ etc.), following a curvature change, were measurable and systematic (figure 7*a–c*), but they appeared to display memory effects and were difficult to interpret by simple arguments. Another observation that could be made is that, although at the entrance of the final straight subsection all anisotropies for NE had values comparable to those for PE, the two sets diverged in that subsection. While possibly spurious, this behaviour is consistent with the observed overshooting, beyond rectilinear shear flow levels, of the turbulence statistics during relaxation of curved flows in straight sections (e.g. in the curved mixing layer of Castro & Bradshaw 1976, and the convex boundary layer of Gillis & Johnston 1983). In general, it appears that negative S promotes anisotropy, while positive S reduces it. The magnitude of the shear stress anisotropy, $m_{uv} = \overline{uv}/q^2$ (figure 7*d*; the significance of the dashed line in this graph will be explained later in this section), showed a much stronger systematic variation, as it clearly increased with decreasing curvature and decreased with increasing curvature (one is reminded of the sign convention for the radius of

https://doi.org/10.1017/S0022112097008185 Published online by Cambridge University Press

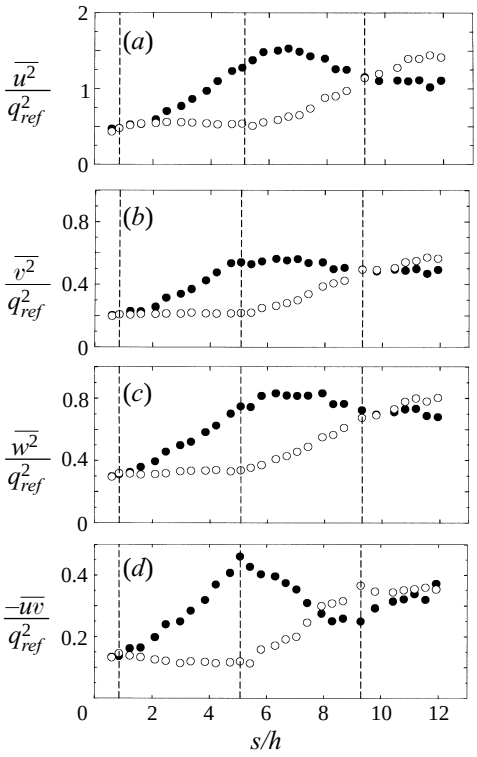


FIGURE 6. Variation of the Reynolds stresses along the centreline for configurations NE (●) and PE (○). (*a*) $\overline{u^2}/q^2{}_{ref}$, (*b*) $\overline{v^2}/q^2{}_{ref}$, (*c*) $\overline{w^2}/q^2{}_{ref}$ and (*d*) $-\overline{uv}/q^2{}_{ref}$. The reference turbulence kinetic energy at the inlet to the first curved subsection was $q^2{}_{ref} = 1.40$ (NE) or 1.46 m^2 s^{-2} (PE). Vertical lines indicate the locations of curvature change.

curvature). The same trends, but even stronger, were displayed by the shear stress correlation coefficient, ρ (figure 7*e*).

The Reynolds stress anisotropies presented above depend on the orientations of the coordinate axes, which, in the present experiments, were variable. A clearer view of the effects of curvature on the turbulence structure would be obtained by observing the evolution of parameters which are invariant to coordinate rotations. Such parameters are the principal stress anisotropies, which, for the present type of two-dimensional mean streams, are equal to

$$m_{1,2} = \frac{m_{uu} + m_{vv}}{2} \pm \left[\left(\frac{m_{uu} - m_{vv}}{2} \right)^2 + m_{uv}^2 \right]^{1/2} \qquad (4.1)$$

$$m_3 = m_{uv}.$$

The anisotropy scalar

$$m^2 = m_{uu}^2 + m_{vv}^2 + m_{ww}^2 + 2m_{uv}^2 \qquad (4.2)$$

is another invariant, although not independent of the principal stress anisotropies. The angle of the maximum principal stress axis with respect to the *s*-axis is

$$\theta_1 = \tfrac{1}{2}\tan^{-1}\frac{-2m_{uv}}{m_{uu} - m_{vv}}. \qquad (4.3)$$

https://doi.org/10.1017/S0022112097008185 Published online by Cambridge University Press

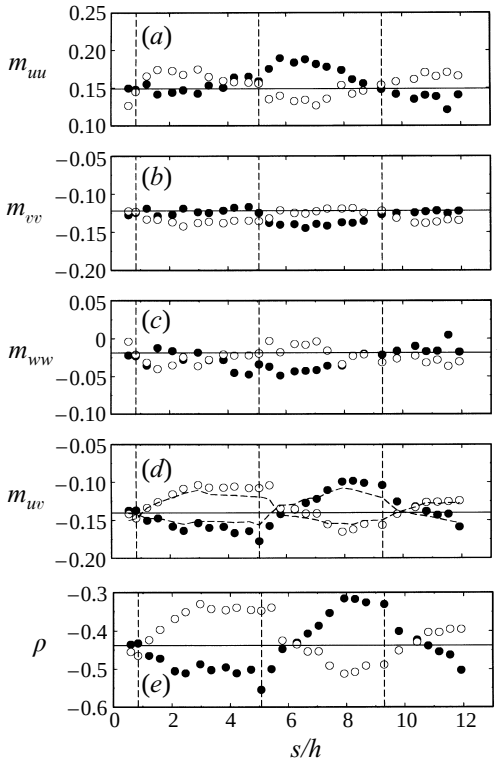


FIGURE 7. Variation of the Reynolds stress anisotropies and the shear stress correlation coefficient along the centreline for configurations NE (●) and PE (○). (*a*) m_{uu}, (*b*) m_{vv}, (*c*) m_{ww}, (*d*) m_{uv} (dashed line corresponds to equation 4.4) and (*e*) ρ. Vertical lines indicate the locations of curvature change.

The developments of the principal anisotropies, the anisotropy scalar and the angle θ_1 along the tunnel centreline are shown in figure 8. Based on the evolution of m^2, one may infer that the overall anisotropy of the flow increased in regions with $S < 0$ and decreased in regions with $S > 0$. The changes in principal stress anisotropies were relatively small, compared to the changes in m_{uv}, suggesting that m_{uv} changed largely due to changes in the orientation of the principal axes. This conclusion is supported by the development of the angle θ_1, which changed by as much as 25% within each subsection. To separate the effects of principal stress orientation from those of their magnitudes, one may use the relationship

$$m_{uv} = \frac{m_1 - m_2}{2} \sin 2\theta_1 \tag{4.4}$$

and assume constant values of the principal stress anisotropies, for example the average value of $m_1 - m_2 \approx 0.4$, corresponding to rectilinear USF. The relevance of the above conjecture was confirmed by observing that the measured m_{uv} was, in general, not very different from its estimates based on the above relationship and plotted as dashed lines in figure 7(*d*). Another worthwhile observation is that changes in θ_1 closely followed changes in the turning angle, s/R_c, at least within a certain region following a change in curvature. This is demonstrated by considering the diagonal lines drawn in figure 8(*d*), which, starting at equilibrium values near the end of each subsection, extend into the subsequent curved subsection with a slope of h/R_c. The hypothetical evolution of θ_1 along these lines would correspond to

https://doi.org/10.1017/S0022112097008185 Published online by Cambridge University Press

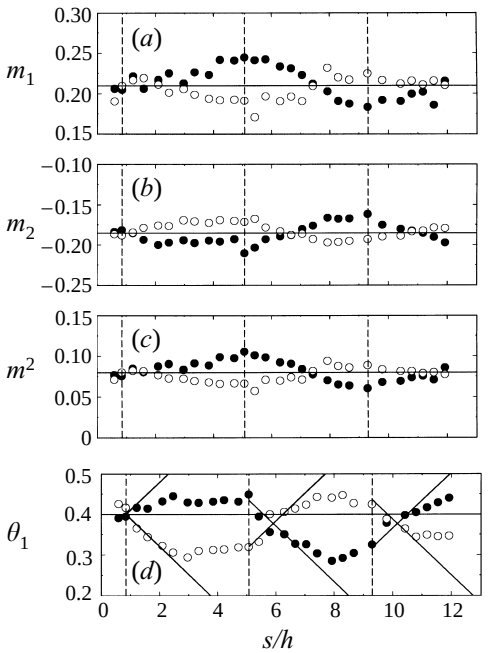


FIGURE 8. Variation of the principal stress anisotropies, the anisotropy scalar and the inclination of the major principal axis along the centreline for configurations NE (●) and PE (○). (*a*) m_1, (*b*) m_2, (*c*) m^2 and (*d*) θ_1 (in rad; inclined solid lines correspond to the angle of rotation of (s, n) directions relative to a fixed Cartesian coordinate system). Vertical lines indicate the locations of curvature change.

the principal axes being fixed to a static Cartesian (i.e. not the present curvilinear) coordinate system. This implies that, at least initially, the coordinate axes may be viewed as rotating away from the principal directions. This behaviour is clearly limited to $\theta_1 < 0.43$, regardless of the direction of flow curvature. Near the end of each subsection, the changes in θ_1 ceased, manifesting that the angles between the principal axes of anisotropy and the principal axes of mean strain rate, which are inclined by $\pm 45^\circ$ with respect to the *s*-direction, approached constant asymptotes. An explanation for the apparent initial rate of change of the turbulence structure upon entering a curved section, due to the reorientation of the coordinate system, will be given in §5.3. The above observation for the present flow differs from the finding of Castro & Bradshaw (1976) that, in a highly curved mixing layer, the observed changes of the shear stress could not be simply attributed to the inherent rotation of the (s, n) coordinate axes.

4.3. *Lengthscales*

The streamwise integral lengthscales were estimated by integrating the corresponding temporal auto-correlation coefficients to their first zero crossings and employing Taylor's frozen flow approximation. The growths of L_{uu}, L_{vv}, and L_{ww}, shown in figure 9, were enhanced for $S < 0$ and suppressed for $S > 0$, with the strongest changes exhibited by L_{vv}, while L_{ww} showed the weakest changes. Although L_{uu} was generally the larger scale, the ordering of the two other scales depended on the history of curvature.

https://doi.org/10.1017/S0022112097008185 Published online by Cambridge University Press

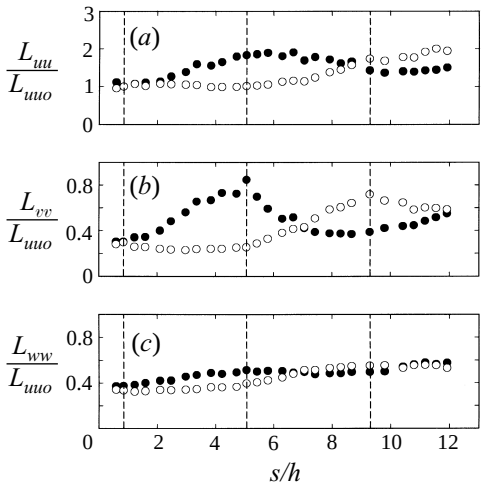


FIGURE 9. Variation of the integral lengthscales along the centreline for configurations NE (●) and PE (○). (*a*) L_{uu}/L_{uuo}, (*b*) L_{vv}/L_{uuo} and (*c*) L_{ww}/L_{uuo}. The reference lengthscale at the inlet to the first curved subsection was $L_{uuo} = 46.4$ (NE) or 49.6 mm (PE). Vertical lines indicate the locations of curvature change.

5. Analysis and discussion of measurements

5.1. *Estimates of streamwise pressure gradient effects*

At this point it is important to examine whether the turbulence development was indeed relatively free of streamwise pressure gradient effects, in conformity with the objective of the present study. Suitable equations for the mean momentum and the Reynolds stresses in curvilinear coordinates and discussion of pressure gradient effects have been presented, among others, by Bradshaw (1973), Castro & Bradshaw (1976), Nakayama (1987) and Baskaran *et al.* (1991). The relevant conclusions of these studies, which also apply to the present configuration, were as follows: (*a*) away from walls, the mean shear would be insensitive to changes in the streamwise pressure gradient; (*b*) the turbulent shear stress is not affected directly by streamwise pressure gradients, as no such term appears in its balance equation; and (*c*) the main contribution of the streamwise pressure gradient to the evolution of the turbulent kinetic energy is the additional production term, termed the 'normal stress production'. According to (*c*), a measure of the relative importance of pressure gradient effects would be the ratio of this production term and the turbulence production by the mean shear, namely

$$F = \frac{-(\overline{u^2} - \overline{v^2})\partial \overline{U}/\partial s}{-\overline{uv}\partial \overline{U}/\partial n}. \tag{5.1}$$

Although this ratio is analogous to the curvature parameter S, there is one important difference in the ways weak curvature and weak pressure gradients affect the turbulence production. Curvature affects the main production term $-(\overline{uv})(\partial \overline{U}/\partial n)$ primarily through its dramatic effect on the shear stress, while the direct production by the additional curvature strain rate, $\overline{U}/R$, may be neglected. In contrast, the shear stress is relatively unaffected by pressure gradients, so that its effects may be altogether negligible, if $F \ll 1$.

Figure 10(*a*) presents the measured mean velocity along the geometric centreline of the test section. The variations of this velocity were relatively small but measurable.

https://doi.org/10.1017/S0022112097008185 Published online by Cambridge University Press

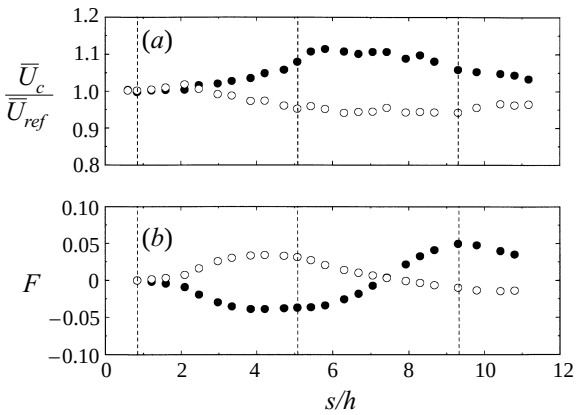


FIGURE 10. Variation of (*a*) the mean velocity ratio, $\overline{U}_c/\overline{U}_{ref}$ and (*b*) the pressure gradient coefficient, F, along the centreline for configurations NE (●) and PE (○). The reference mean velocity was $\overline{U}_{ref} = 10.05$ (NE) or 10.30 m s^{-1} (PE).

They can be attributed to curvature changes and unequal growths of the boundary layers along the four walls of the test section. The streamwise derivative of the mean velocity was estimated by polynomial fitting to the measurements and was used, together with local measurements of the Reynolds stresses and the mean shear rate, to estimate the variation of the parameter F, shown in figure 10(*b*). Even when doubled to account for possible streamline divergence, this parameter never exceeded 10%, which is sufficient assurance for disregarding pressure gradient effects. Significant pressure gradients cannot be generated in the present type of flow except deliberately, as for example in the experiments of Akbary (1997), in which substantial flow acceleration was superimposed on curved USF by reducing gradually the test section's height.

Our estimates corroborate the assessment of Bandyopadhyay & Ahmed (1993) that curvature effects dominated those of pressure gradient for their boundary layers subjected to successive convex–concave and concave–convex wall surface curvatures. In contrast, pressure gradients were much stronger in other curved flow experiments, for example those by Nakayama (1987) and Baskaran *et al.* (1991), in which both the pressure gradient parameter, F, and the curvature parameter, S, attained magnitudes of the order of 1.

5.2. *The turbulence in 'fully developed' regions*

One of the most important conclusions reached by HT for fully developed, curved USF was that, for relatively weak curvature effects ($-0.20 < S < 0.20$), the shear stress anisotropy, m_{uv}, could be approximately described by the linear relationship

$$m_{uv} \approx -0.14(1 - 3.0S), \tag{5.2}$$

while, for dominant curvature effects ($S \to \pm\infty$), $m_{uv} \to 0.25$. The present measurements of m_{uv} in the downstream halves of each subsection were consistent with the above relationship, indicating that the turbulence structure in these regions approached self-similarity. The growth of the turbulent kinetic energy in each subsection, normalized by its value, q_i^2, at the entrance to that subsection, has been plotted in figure 11 against the total strain within the same subsection, $\Delta\tau = \tau - \tau_i$, where τ_i is the total strain at the entrance to that subsection. The solid lines, passing through the

https://doi.org/10.1017/S0022112097008185 Published online by Cambridge University Press

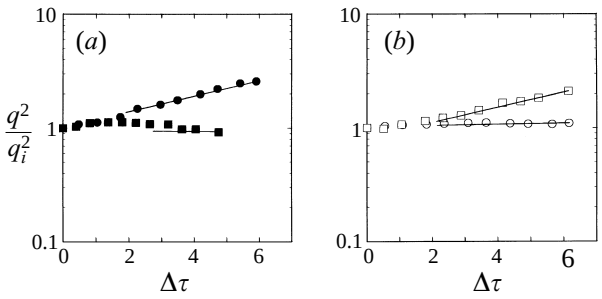


FIGURE 11. Evolution of the turbulent kinetic energy within the curved subsections for configurations (*a*) NE and (*b*) PE. The corresponding values of the curvature parameter were $S \approx -0.049$ (●), 0.060 (■), 0.047 (○) and −0.047 (□). The solid lines represent equation (5.3).

last measurement points, represent asymptotic exponential evolution of the type

$$\frac{q^2}{q_\infty^2} = \mathrm{e}^{\kappa_{q\infty}(\tau-\tau_\infty)} \tag{5.3}$$

where the coefficient κ_{q_∞} was computed from an empirical expression given by HT and the subscript ∞ refers to a far downstream location, which is non-essential for the present purposes. With the possible exception of the $S = 0.060$ case, the data in the downstream half of each curved subsection appear to be compatible with this equation, thus further confirming the existence of 'fully developed' regions. The upstream halves, where the flow structure was adjusting to a change in curvature and deviations from these relations were significant, can be categorized as 'entrance' regions. The presence of these two regions is also confirmed by the development of m_{uv} in each subsection. In all cases, there were entrance regions, in which a parameter adjusted, and fully developed regions, where the same parameter approached the values predicted by the asymptotic expressions of HT, in which the nominal values of S in the corresponding sections were used.

Within each fully developed region, the dynamic process of production, evolution and destruction of turbulent eddies can be characterized by the average lifetime of the energy-containing eddies, $t_u = q^2/\epsilon$. This timescale should be related to the local values of the two externally imposed timescales, namely the inverse mean shear rate, $t_s = |\partial\overline{U}/\partial n|^{-1}$, and the turning rate, $t_c = R_c/\overline{U}_c$. For small $|S|$, t_u should be proportional to t_s, while, for large $|S|$, it should be proportional to t_c. Now, let us focus on cases with zero and small $|S|$. It has been well documented (e.g. by Sreenivasan 1985 and Tavoularis & Karnik 1989) that, in rectilinear USF as well as in outer boundary layers and other shear flows, the ratio $t_u/t_s = c_u$ is a constant of order 10. For the present purposes, the turbulent kinetic energy dissipation rate, ϵ, was estimated as the balance of the other measureable terms in the simplified equation (2.2). The uncertainty in ϵ and the corresponding uncertainty in t_u are, roughly, $\pm 30\%$. The small-$|S|$ results of HT as well as the present measurements are compatible with a linearized relationship of the form

$$t_u/t_s \approx c_u(1 - 2.2S) \tag{5.4}$$

with c_u a constant of order 10. This implies that curvature with $S < 0$ tends to prolong the life of the energy-containing eddies and curvature with $S > 0$ tends to shorten it.

In summary, the present measurements in the downstream portions of the two

https://doi.org/10.1017/S0022112097008185 Published online by Cambridge University Press

curved sections essentially reproduce the findings of HT for small values of $|S|$. In the following section, we shall discuss the main subject of the present study, namely the rate of adjustment of the turbulence to curvature changes.

5.3. *The rate of adjustment to curvature changes*

The evolution of a general curved shear flow seems to be far too complex to be described by relatively simple means, because, in the presence of continuously changing curvature, the local timescale of the turbulence eddies would likely depend strongly on the past states of the flow. Therefore, we shall only attempt to analyse the case of a turbulent flow which, starting from a self-similar state that developed under the influence of uniform shear and curvature, underwent a stepwise change in mean streamline curvature, and was then allowed to achieve a new self-similar, fully developed state. In this case, in addition to the local turbulent eddy lifetime, t_u, one should also consider a timescale representing the process of turbulence adjustment from an old to a new structural state. This timescale applies to a volume of fluid convected along a mean streamline and travelling with the mean convection speed. If the turbulence is viewed in a stationary frame, it is more appropriate to use a development length, corresponding to the minimum distance (along the mean streamline) between locations with the old and the new structural states. Among the various parameters that can be used in determining structural adjustment, the quantity m_{uv} was found to be the most sensitive to curvature changes. In order to accommodate cases with different initial and final states, we shall consider the variation of this quantity in the reduced form

$$\delta m = \frac{m_{uv} - m_{uvo}}{m_{uv\infty} - m_{uvo}}, \tag{5.5}$$

where the subscript o indicates the initial structure at the location of curvature change and the subscript ∞ indicates the far downstream fully developed structure.

Figure 12 plots δm versus τ for the six present cases, including transitions from straight to curved flow, from convex to concave flow, or vice versa, and from curved to straight flow. The scatter is appreciable, yet all sets of data appear to collapse in a cluster. The observed scatter is consistent with uncertainty estimates for δm. The uncertainty of m_{uv}, based on the estimates in §3.2, is 8.5%, but the uncertainty in the asymptotic values of m_{uv} could be higher, because of the uncertainty in establishing the fully developed regions. Taking the latter to be 17%, and using as typical values $m_{uv} = 0.12$, $m_{uvo} = 0.15$, and $m_{uv\infty} = 0.10$, one may estimate a typical 95% confidence level uncertainty in δm as ± 0.3. Also shown in figure 12, as a dashed line, is the exponential expression

$$\delta m = 1 - \mathrm{e}^{-\Delta\tau/T_d}, \tag{5.6}$$

which seems to describe fairly well the evolution of δm, thus suggesting that structural adjustment to a step change in curvature may be roughly modelled by the step response of a first-order linear system. The dimensionless time constant of the optimal exponential curve was $T_d \approx 1.5$, while most of the data were bracketed by exponential curves having $T_d \approx 1.0$ and 2.25. This implies that δm would reach 95% of its asymptotic value within a convection time of $4.5t_s$, or a streamwise distance of $4.5/k_s$. This adjustment time is comparable to t_u and to values suggested by several investigators as required for the full development of rectilinear USF and for the adjustment of USF structure following a contraction (Sreenivasan 1985). Therefore, one may conclude that, at least for relatively small $|S|$, the mean shear is the primary factor in determining the rate of adjustment to geometrical changes.

https://doi.org/10.1017/S0022112097008185 Published online by Cambridge University Press

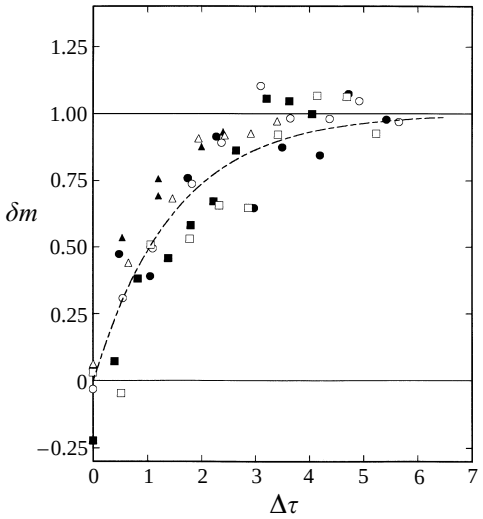


FIGURE 12. Adjustment of the normalized shear stress anisotropy difference, δm, following a step change in curvature for the configurations NE (solid symbols) and PE (open symbols); circles indicate measurements in the first curved subsection, squares in the second curved subsection and triangles in the final straight subsection; the dashed line is an exponential curve with a dimensionless time constant of 1.5.

Figure 12 was examined carefully for any hints for a possible dependence of T_d on the strength of curvature and its change. In all three cases, data sets corresponding to changes with nearly opposite S appeared to collapse. This may be interpreted as evidence that the sign of S is not important. Based on the present experimental evidence, one may reasonably conclude that, for a given geometrical configuration and for small values of the curvature parameter, S, the dimensionless rate of adjustment to curvature changes is roughly independent of S. This implies that the actual adjustment time scales with the inverse mean shear rate, which is consistent with the fact that, in this class of flows, mean shear is the main turbulence production mechanism, imposing its timescale on all related events. Therefore, for a fixed mean shear rate, a flow would adjust to arbitrary small changes of mean radius of curvature in approximately the same time. On the other hand, for a given mean streamline radius of curvature, a flow with higher shear (i.e. lower $|S|$, relatively weaker curvature) would likely adjust to curvature changes faster than a flow with lower shear (i.e. higher $|S|$, relatively stronger curvature).

This empirically found exponential form of the parameter δm can be used to explain the observed initial changes in the shear stress anisotropy, following a stepwise change in curvature. Towards this purpose, one may expand the exponential expression in equation (5.6) into a power series and retain only the linear term. Further using the asymptotic expression (5.2) and some algebraic manipulations, one may easily estimate that, for small s (measured from the location of curvature change),

$$m_{uv} \approx m_{uvo} + \frac{0.42}{T_d}\left(\frac{1}{R_{c\infty}} - \frac{1}{R_{co}}\right)\Delta S, \tag{5.7}$$

which clearly indicates that the initial rate of change of m_{uv} would depend only on the change of the radius of curvature and it would be independent of the mean shear! This result explains the initial variation of m_{uv} in the present experiments (figure 7*d*

https://doi.org/10.1017/S0022112097008185 Published online by Cambridge University Press

and can be easily extended to explain the initial change in the apparent inclinations of the principal stress axes (e.g. as shown in figure 8*d*). In fact, HT have also observed that the initial rate of change of m_{uv} in their experiments scaled with the radius of curvature (see their figure 13), although they attributed this effect to the large values of S. In the light of the present analysis, one may put forward the hypothesis that, no matter how weak or strong the shear is, the structural changes occur at an initial rate which scales with the radius of curvature but reach their asymptotes after a distance which scales with the parameter k_s^{-1}.

6. Interpretation of curvature effects on turbulent boundary layers using USF results

In the present section, measurements on turbulent boundary layers over curved walls will be analysed in light of the conclusions derived from the curved USF. It will be shown not only that the two types of flows bear strong qualitative similarities, but, also, that some of their important features can be predicted by the same semi-empirical formulas. As in the USF case, we shall first analyse the asymptotic structure of turbulent boundary layers subjected to prolonged uniform curvature and, then, we shall deal with the boundary layer adjustment to stepwise changes of curvature.

6.1. *Asymptotic structure of curved boundary layers*

In turbulent boundary layers, both parameters S and m_{uv} vary across and along the layer. Concave wall curvature tends to increase the growth rate of the boundary layer thickness above the plane wall level, thus increasing the streamwise variation of S, while convex wall curvature has the opposite effects. Furthermore, concave boundary layers are known to exhibit spanwise variation of the mean flow and the turbulence parameters, because of quasi-steady longitudinal vortices, which are believed to depend strongly on upstream non-uniformities (Barlow & Johnston 1988). Nevertheless, we have confirmed that the asymptotic USF relationship (4.4), for the shear stress anisotropy, also holds approximately for the outer fully turbulent (i.e. non-intermittent) regions of boundary layers over convex walls with a uniform radius of curvature and following sufficient development length. Measurements in outer layers over concave walls are in poor agreement both with each other and with predictions based on equation (5.2) (figure 13).

In order to further explore the apparent analogy between USF and curved turbulent boundary layers, one needs an analytical expression for the velocity profile in the latter. For simplicity, it will be assumed that the outer boundary layer profile can be approximated by the power law,

$$\frac{\overline{U}}{\overline{U}_\infty} = \xi^{1/p} \tag{6.1}$$

where $\xi = n/\delta$. The applicability of a power law with $p \approx 7$, to plane boundary layers has been well documented. We have also successfully fitted power laws with p in the range 4.5 to 4.8 to the data of Gillis & Johnston (1983) for fully developed boundary layers over convex walls. On the other hand, the applicability of a power law to concave layers is rather uncertain, although a power law with $p \approx 7.9$ seemed to describe the data of Ramaprian & Shivaprasad (1977) and Shivaprasad & Ramaprian (1978).

Considering thin, outer layers whose mean velocity can be described by a power

https://doi.org/10.1017/S0022112097008185 Published online by Cambridge University Press

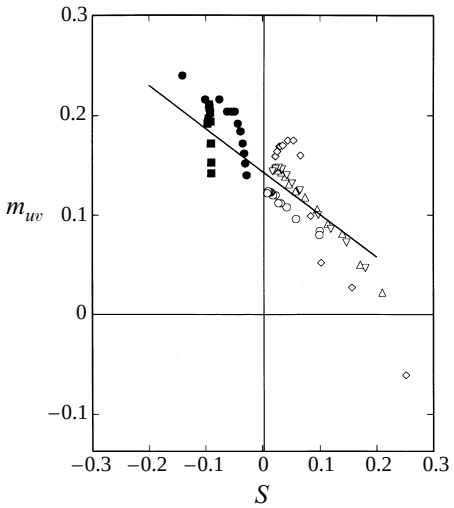


FIGURE 13. Comparison of measured profiles of the shear stress anisotropy in curved boundary layers with a simple prediction using USF results (—— , equation (5.2)). Convex layers: △, Gillis & Johnston (1983), $\delta/R_w = 0.10$; ▽, Gillis & Johnston (1983), $\delta/R_w = 0.05$; ○, Ramaprian & Shivaprasad (1977) and Shivaprasad & Ramaprian (1978); ◇, So & Mellor (1973). Concave layers: ●, Ramaprian & Shivaprasad (1977) and Shivaprasad & Ramaprian (1978); ■, Barlow & Johnston (1988).

law, one can easily show that the curvature parameter can be expressed as

$$S = \pm p \frac{\xi}{(R_w/\delta) \pm \xi} \approx \pm p\xi \frac{\delta}{R_w} = \pm p \frac{n}{R_w} \tag{6.2}$$

which shows clearly that the relative strength of curvature increases with distance from the wall. Substituting equation (6.2) into equation (5.2), and using a value of $p = 4.7$, one may derive the following expression for the shear stress anisotropy profile across convex boundary layers:

$$m_{uv} \approx 0.14 \left(1 - 14.1 \frac{\delta}{R_w} \xi\right). \tag{6.3}$$

This is perfectly consistent with Gillis & Johnston's (1983) empirical observation that shear stress profiles in convex layers collapse when plotted *vs.* n/R_w. Using, as typical, the values of S and m_{uv} at $\xi = 0.5$, one may conclude that

$$(m_{uv})_{0.5} \approx 0.14 \left(1 - 7.0 \frac{\delta}{R_w}\right), \tag{6.4}$$

which reproduces Bradshaw's (1973) conclusion that curvature appears to affect turbulence production as if its magnitude were amplified by a factor of the order of 10. Equation (6.3) can also be used to estimate the thickness of the 'active shear stress layer' (namely the distance from the wall at which the shear stress vanishes) as

$$\xi_o \approx \frac{1}{3p\delta/R_w} \quad \text{or} \quad \frac{n_o}{R_w} \approx 0.07 \tag{6.5}$$

which is independent of the initial boundary layer thickness, as Gillis & Johnston (1983) rightly observed. One may also observe that, according to equation (6.5), the shear stress would vanish at a location where $S \approx 0.33$.

https://doi.org/10.1017/S0022112097008185 Published online by Cambridge University Press

We shall close this section with another example of the usability of USF results in the prediction of boundary layer properties. Gillis & Johnston (1980) claimed that, in the low-shear-stress outer region of the convex boundary layer, the turbulence would be essentially isotropic and used the isotropic turbulence decay law to predict the evolution of its kinetic energy. HT have demonstrated that, in curved USF, the turbulence is highly anisotropic, even where the shear stress vanishes. Therefore, an exponential kinetic energy evolution law, like equation (5.3), would likely be more appropriate than the isotropic power decay law. The total strain, τ, from the start of curvature can be expressed as

$$\Delta\tau \approx \frac{1}{p\xi}\frac{\Delta S}{\delta}. \tag{6.6}$$

If, for simplicity, one substitutes the estimated values of S and ξ at the zero-shear-stress point into the expression provided by HT for the coefficient κ_q, one may derive the decay law

$$\frac{q^2}{q_o^2} = \mathrm{e}^{-0.80\Delta s/R_w} \tag{6.7}$$

which fits the Gillis & Johnston (1980) data at least as well as their isotropic expression.

6.2. *Adjustment to a step change in curvature*

The rate of adjustment of boundary layers to start or removal of curvature has been examined by several investigators, but both the measurements and their interpretations vary and often contradict each other. Part of the discrepancies may be due to differences in geometries and experimental conditions, because the boundary layer structure is sensitive to many factors. One of the conclusions that seem to find general acceptance (e.g. see Alving & Smits 1986 and Smits & Wood 1985) is that the turbulence attains self-preservation much faster near the wall than in the outer layer. This is perfectly consistent with the present finding that, for a given curvature change, the adjustment time would be inversely proportional to the mean shear: the streamline radius of curvature is essentially constant across a thin layer, while the mean shear decreases rapidly with distance from the wall. In other words, both USF and boundary layer measurements have demonstrated that the response to curvature would be slower at locations where the mean shear is relatively weaker.

The quantitative description of the adjustment time in boundary layers faces the difficulties of continuous variation of properties across the flow and the fact that different properties adjust at different rates. In boundary layers, as well as in USF, it is the Reynolds stress anisotropies that adjust the fastest, with the shear stress anisotropy being the most sensitive among all others (Gillis & Johnston 1983; Alving *et al.* 1990). For this reason, we have chosen the shear stress anisotropy as an indicator of adjustment. For an order of magnitude analysis, one could assume a power law profile, which describes well plane and convex outer layers and at least some concave layers. Then, the dimensionless adjustment length, $\Delta s_d/\delta$, can be calculated as

$$\frac{\Delta s_d}{\delta} \approx p\xi\Delta\tau_d \tag{6.8}$$

where $\Delta\tau_d$ is the dimensionless adjustment time, estimated from the present measurements to be about 4.5. Further considering realistic values of p in the range of 4.5 to 5.0 for convex layers, about 7.0 for plane layers and somewhat higher for concave layers, and taking the mid-layer ($\xi = 0.5$) as a representative location, one

https://doi.org/10.1017/S0022112097008185 Published online by Cambridge University Press

reproduces the familiar value of an adjustment length of the order of 10δ, proposed by Bradshaw (1973) and later confirmed by many other investigators. Interestingly enough, the above expression even discriminates between the different types of boundary layers through differences in their values of p. Despite the apparent qualitative success of the simplistic empirical expression (6.8), one must concede that the available boundary layer measurements are subjected to effects (e.g. non-equilibrium and three-dimensional effects) that cannot be accommodated by relationships based on USF-type flows.

7. Conclusions

The present study is the latest in a series of mainly experimental investigations of uniformly sheared flows (USF), which have, in our opinion, further established their utility not only as a simplified paradigm of active turbulence, but also as a tool for producing and testing results useful in the understanding and prediction of far more complex turbulent flows. USF are known to employ considerable theoretical and experimental approximations, yet the previous and present studies have proved that the main effects of shearing and streamline curvature can be identified and described, both qualitatively and quantitatively (for certain purposes), from USF results.

For the present experiments, USF were allowed to develop in a sequence of straight and curved wind tunnel sections. A first conclusion was that, sufficiently far downstream from the locations of stepwise changes in curvature, the turbulence reached asymptotic structures, all features of which were independent of the upstream histories of the flows and in excellent agreement with measurements of Holloway & Tavoularis (1992) in curved sections. HT's asymptotic expressions for the dependence of the dimensionless shear stress anisotropy and the growth rate of the turbulent kinetic energy upon the curvature parameter, S, were confirmed and proved to apply, approximately, not only to USF but also to the outer regions of curved turbulent boundary layers.

The main objective of the present work, namely the description of the turbulence adjustment to curvature changes, has also been met, at least for the 'weak' curvature range. All present measurements appear compatible with an exponential adjustment of the shear stress anisotropy for which the 'time constant' is inversely proportional to the mean shear rate and approximately independent of the flow curvature before and after the change. Surprisingly, this simple model makes reasonable predictions of the turbulent boundary layer adjustment to wall curvature changes.

Financial support for the above research was provided by the Natural Sciences and Engineering Research Council of Canada.

REFERENCES

Akbary, H. 1997 Effects of extra strain rates on uniform shear flow and their relevance to impeller flows. PhD thesis, University of New Brunswick, Fredericton, Canada.

Alving, A. E. & Smits, A. J. 1986 The recovery of a turbulent boundary layer from longitudinal curvature. *AIAA Paper* 86-0435.

Alving, A. E., Smits, A. J. & Watmuff, J. H. 1990 Turbulent boundary layer relaxation from convex curvature. *J. Fluid Mech.* **211**, 529–556.

Bandyopadhyay, P. R. & Ahmed, A. 1993 Turbulent boundary layers subjected to multiple curvatures and pressure gradients. *J. Fluid Mech.* **246**, 503–527.

https://doi.org/10.1017/S0022112097008185 Published online by Cambridge University Press

Barlow, R. S. & Johnston, J. P. 1988 Structure of a turbulent boundary layer on a concave surface. *J. Fluid Mech.* **191**, 137–176.

Baskaran, V., Smits, A. J. & Joubert, P. N. 1987 A turbulent flow over a curved hill. Part 1. Growth of an internal boundary layer. *J. Fluid Mech.* **182**, 47–83.

Baskaran, V., Smits, A. J. & Joubert, P. N. 1991 A turbulent flow over a curved hill. Part 2. Effects of streamline curvature and streamwise pressure gradient. *J. Fluid Mech.* **232**, 377–402.

Bradshaw, P. 1973 Effects of streamline curvature on turbulent flow. *AGARDograph* 169.

Castro, I. P. & Bradshaw, P. 1976 The turbulence structure of a highly curved mixing layer. *J. Fluid Mech.* **73**, 265–304.

Corrsin, S. 1963 Turbulence: experimental methods. In *Hanbuch der Physik* (ed. S. Flügge & C. Truesdell), vol. 8/2, pp. 523–590. Springer.

Gatski, T. B. & Savill, A. M. 1989 An analysis of curvature effects for the control of wall-bounded shear flows. *AIAA*-89-1014.

Gibson, M. M., Verriopoulos, C. A. & Vlachos, N. S. 1984 Turbulent boundary layer on a mildly curved convex surface: Part 1, Mean flow and Turbulence measurements. *Exps. Fluids* **2**, 17–24.

Gillis, J. C. & Johnston, J. P. 1980 Experiments on the turbulent boundary layer over convex walls and its recovery to flat-wall conditions. In *Turbulent Shear Flows* (ed. L. J. S. Bradbury *et al.*), vol. 2, pp. 116–128. Springer.

Gillis, J. C. & Johnston, J. P. 1983 Turbulent boundary-layer flow and structure on a convex wall and its redevelopment on a flat wall. *J. Fluid Mech.* **135**, 123–153.

Harris, V. G., Graham, J. A. & Corrsin, S. 1977 Further experiments in nearly homogeneous turbulent shear flow. *J. Fluid Mech.* **81**, 657–687.

Hoffman, P. H., Muck, K. C. & Bradshaw, P. 1985 The effects of concave surface curvature on turbulent boundary layers. *J. Fluid Mech.* **161**, 371–403.

Holloway, A. G. L. & Tavoularis, S. 1992 The effects of curvature on sheared turbulence. *J. Fluid Mech.* **237**, 569–603 (referred to herein as HT).

Holloway, A. G. L. & Tavoularis S. 1993 Effects of curvature on the spectra of sheared turbulence. In *Turbulent Shear Flows* (ed. F. Durst *et al.*), vol. 8, pp. 383–401. Springer.

Karnik, U. & Tavoularis, S. 1987 Generation and manipulation of uniform mean shear with the use of screens. *Exps. Fluids* **5**, 247–254.

Muck, K. C., Hoffmann, P. H. & Bradshaw, P. 1985 The effect of convex surface curvature on turbulent boundary layers. *J. Fluid Mech.* **161**, 347–369.

Nakayama, A. 1987 Curvature and pressure-gradient effects on a small-defect wake. *J. Fluid Mech.* **175**, 215–246.

Ramaprian, B. R. & Shivaprasad, B. G. 1977 Mean flow measurements in turbulent boundary layers along mildly curved surfaces. *AIAA J.* **15**, 189–196.

Shivaprasad, B. G. & Ramaprian, B. G. 1978 Turbulence measurements in boundary layers along mildly curved surfaces. *Trans. ASME*: *J. Fluids Engng* **100**, 37–46.

Smits, A. J. & Wood, D. H. 1985 The response of turbulent boundary layers to sudden perturbations. *Ann. Rev. Fluid Mech.* **17**, 321–358.

Smits, A. J., Young, S. T. B. & Bradshaw, P. 1979 The effect of short regions of high surface curvature on turbulent boundary layers. *J. Fluid Mech.* **94**, 209–242.

So, R. M. C. & Mellor, G. L. 1973 Experiments on convex curvature effects in turbulent boundary layers. *J. Fluid Mech.* **60**, 43–62.

Sreenivasan, K. R. 1985 The effect of contraction on a homogeneous turbulent shear flow. *J. Fluid Mech.* **154**, 187–213.

Tavoularis, S. & Karnik, U. 1989 Further experiments on the evolution of turbulent stresses and scales in uniformly sheared turbulence. *J. Fluid Mech.* **204**, 457–478.

Wyngaard, J. C. 1969 Spatial resolution of the vorticity meter and other hot-wire arrays. *J. Phys.* E **2**, 983–987.

https://doi.org/10.1017/S0022112097008185 Published online by Cambridge University Press